Published in final edited form as:
Magn Reson Med. 2004 December ; 52(6): 1234–1238.

Imaging Therapeutic Response in Human Bone Marrow Using Rapid Whole-Body MRI

Douglas Ballon[1,2,3,4,*], **Richard Watts**[1,2], **Jonathan P. Dyke**[1,2], **Eric Lis**[4], **Michael J. Morris**[5], **Howard I. Scher**[5], **Aziz M. Ulug**[1], and **Ann A. Jakubowski**[5]

1 *Department of Radiology, Weill Medical College of Cornell University, New York, New York*

2 *Citigroup Biomedical Imaging Center, Weill Medical College of Cornell University, New York, New York*

3 *Department of Medical Physics, Memorial Sloan-Kettering Cancer Center, New York, New York*

4 *Department of Radiology, Memorial Sloan Kettering Cancer Center, New York, New York*

5 *Department of Medicine, Memorial Sloan-Kettering Cancer Center, New York, New York*

Abstract

Whole-body imaging of therapeutic response in human bone marrow was achieved without introduced contrast agents using diffusion-weighted echo-planar magnetic resonance imaging of physiologic water. Bone marrow disease was identified relative to the strong overlying signals from water and lipids in other anatomy through selective excitation of the water resonance and generation of image contrast that was dependent upon differential nuclear relaxation times and self-diffusion coefficients. Three-dimensional displays were generated to aid image interpretation. The geometric distortion inherent in echo-planar imaging techniques was minimized through the acquisition of multiple axial slices at up to 12 anatomic stations over the entire body. Examples presented include the evaluation of therapeutic response in bone marrow during cytotoxic therapy for leukemia and metastatic prostate cancer and during cytokine administration for marrow mobilization prior to stem cell harvest.

Keywords

tumor therapy; cancer; hematopoiesis; diffusion

The assessment of hematopoiesis in humans is generally achieved through analysis of a bone marrow biopsy and/or aspirate from either the iliac crest or the sternum, combined with examination of the peripheral blood (1). Biopsy or aspirate specimens typically have a sample volume of no more than 0.1 cm^3 compared to a potential total active marrow volume of greater than 1000 cm^3. Furthermore, while many hematologic disorders are known to diffusely infiltrate the axial bone marrow, the overall distribution of disease can be heterogeneous on a length scale that precludes an accurate assessment via an aspirate or biopsy from a single site. In cases of focal bone marrow metastases from a known primary tumor, the direct assessment of disease is even more difficult since the tumors are often inaccessible to all but a surgical biopsy.

---

*Correspondence to: Douglas J. Ballon, Weill Cornell Medical College, 1300 York Avenue Box 234, New York, NY 10021. E-mail: djb2001@med.cornell.edu.

Portions of this work were presented at the International Society for Magnetic Resonance in Medicine Eleventh Annual Scientific Meeting (2003).

Perhaps more important than the evaluation of tumor burden is the concept of noninvasive therapeutic monitoring (2). Increasingly, it has been suggested that patient management and treatment outcome might be affected if the efficacy of chemotherapeutic agents could be determined via imaging methods within days or even hours after the initiation of therapy. Earlier recognition of ineffective therapy, for example, would permit more rapid change in treatment programs and perhaps avoid associated toxicities. Currently, therapeutic monitoring of hematologic disease requires multiple invasive bone marrow procedures with associated patient discomfort. For metastatic disease in bone, ^{99m}Tc bone scans are a sensitive method of tumor evaluation (3). However, bone scans are only an indirect measure of tumor activity by virtue of the associated osteoblastic reaction and can in certain cases even suggest disease progression within the first month after initiation of therapy in patients that ultimately demonstrate a good response.

The methods described below allow for a whole-body assessment of human bone marrow in under 20 min at a spatial resolution of 75 mm^3. This was sufficient for observing a therapeutic response in a number of examples. The techniques can be combined with established two-dimensional magnetic resonance methods for bone marrow evaluation and offer a rapidly obtained, three-dimensional data set that can readily be compared with a bone scan or positron emission tomogram if desired. Visualization of the three-dimensional data set is dependent upon the fact that bone marrow disease can be segmented from images of the pelvis and abdomen using strong spin-spin relaxation time and water self-diffusion-weighted image contrast along with high-quality lipid suppression. The attainable signal-to-noise ratios per unit voxel have previously been shown to be up to five times more sensitive to the presence of leukemic blasts in acute lymphocytic, chronic lymphocytic, and chronic myelogenous leukemia than to detection of normal hematopoietic bone marrow (4). Specifically, signal intensities are related to the apparent water fraction, as well as proton spin-spin relaxation values and self-diffusion coefficients of water in bone marrow as

$$S \propto W_a e^{-(TE/T_2 + bTr\mathbf{D}*/3)}. \quad [1]$$

Here W_a is the apparent water fraction, defined according to a three-point Dixon reconstruction of the separate water and fat signals in bone marrow as $W/(W + F)$ (5). The apparent water fraction has been shown to vary linearly with the percentage cellularity in intact bone marrow (6). Also in Eq [1], TE is the echo time, T_2 is the spin-spin relaxation time, b is the diffusion weighting factor defined by the Stejskal–Tanner relation (7), and Tr**D*** represents the trace of the apparent diffusion coefficient tensor **D***. Finally, the methods require no introduced contrast agents or any invasive procedure. The subject is simply required to lie still within the magnet for a series of 60- to 80-sec intervals over the course of the examination.

Three examples are presented in this paper to illustrate the potential utility of the methods for imaging therapeutic response in bone marrow. They are, respectively, from a healthy volunteer receiving a white blood cell growth factor for bone marrow stem cell mobilization prior to leukopheresis harvesting, from a patient who was treated for acute myelogenous leukemia and achieved a hematologic remission 20 days after the initiation of therapy, and from a patient with metastatic prostate cancer who exhibited a mixed response to therapy over a 3-month period.

METHODS

All image data were acquired on a 1.5-T whole-body magnetic resonance imaging system (GE Medical Systems, Milwaukee, WI). A fast gradient echo localizing pulse sequence was followed by either a T_1-weighted sequence, with a repetition time of 500 msec and an echo time of 20 msec, or a T_2-weighted inversion recovery (STIR) sequence, with a repetition time

of 6.9 sec, an echo time of 51 msec, and an inversion time of 150 msec covering the axial skeleton (8). A single-shot echo-planar acquisition scheme was then employed that included a spatial–spectral selective radiofrequency pulse sequence to limit excitation to the water resonance while discriminating against signals from mobile lipids (9,10). Data were acquired in up to 12 series, each containing 30 contiguous axial slices with a field of view equal to 36 × 36 cm and a matrix size of 128 × 80 per slice. The slice thickness was 6 mm and slices were acquired in interleaved fashion at a bandwidth of 131 kHz. The pulse sequence repetition time was 10 sec, and the echo time was 100 msec. Diffusion weighting was accomplished using two 32-msec, 2.2 G/cm gradient pulses initiated 40 msec apart that straddled the 180° radiofrequency pulse, resulting in a diffusion weighting factor of $b = 1000$ sec/mm^2. The diffusion pulses were individually applied along each spatial axis in three sequential applications of the pulse sequence. In addition a set of images was obtained with no diffusion weighting for each series. The total time required for scanning a single series of images was 80 sec. Beginning with the first axial series covering the brain, the five most inferior slices were overlapped with the five most superior slices from the next series to allow flexibility in the choice of images at the edges of the field of view.

In certain cases it was of interest to determine the water T_2 values, apparent water fractions, and self-diffusion coefficients from regions of interest within the bone marrow. A three-point Dixon method was used for calculation of both T_2 values and the apparent water fraction as described previously (11), and the self-diffusion coefficients were calculated as described below.

Image postprocessing for each slice included homodyne reconstruction of the raw data followed by zero-filling to a 256 × 256 matrix and a distortion correction for nonlinearity in the magnetic field gradients. The diffusion images obtained along each spatial axis for each slice were combined according to

$$S(x_i, y_i) = [S_x(x_i, y_i)S_y(x_i, y_i)S_z(x_i, y_i)]^{1/3}, \quad [2]$$

where $S_j(x_i,y_i)$ represents the image intensity at a point (x_i,y_i) obtained with the diffusion gradients applied along the jth axis. Combining the images in this way generated contrast that was dependent upon the trace of the diffusion tensor according to Eq. [1]. From the $b = 0$ and $b = 1000$ sec/mm^2 images an estimate of apparent self-diffusion coefficients was obtained by first selecting regions of interest encompassing approximately 1–3 cm^3 in the axial images and then applying Eq. [1] directly on a voxel-by-voxel basis. The values and statistical errors quoted for $D^* = \mathrm{Tr}\mathbf{D}^*/3$ in this paper are the means and standard deviations from the means calculated for the regions of interest.

The trace images for all slices in all series were stored in a three-dimensional array using the Interactive Data Language (Kodak, Rochester, NY). An inverse grayscale intensity scale was applied to the data sets for visual interpretation, which conforms to a typical standard for other whole-body methods such as PET or bone scans. The three-dimensional data sets could be viewed along any axis as maximum intensity projections and were displayed in a cine loop format with each frame representing 10° of image rotation along the superior–inferior direction in the patient frame of reference. In order to discriminate against subcutaneous fat left unsuppressed by the spatial–spectral excitation pulse, elliptical step function masks were typically applied to the axial images.

The imaging study protocol was reviewed and approved by Institutional Review Boards at both Memorial Sloan-Kettering Cancer Center and New York–Presbyterian Hospital–Weill Cornell Medical College. Patients were entered into the imaging studies after informed consent was obtained. Chemotherapeutic agents and growth factor were administered as part of separate

clinical protocols and not as part of the imaging study described herein. Images were acquired from a total of six patients including the three studied for therapeutic response. Three patients with chronic myelogenous leukemia underwent single studies during the development phase of the methods. These patients were chosen for the strong signal intensities on T_2-and diffusion-weighted images and expanded active marrow volume that often accompanies this disease.

RESULTS

An example of a maximum intensity projection image from a whole-body data set is presented in Fig. 1 from a normal adult volunteer who was receiving granulocyte colony-stimulating factor (G-CSF) prior to a peripheral blood stem cell harvest. Figure 1a was obtained on Day 0 and Fig. 1b on Day 5 during 8 μg/kg of G-CSF administered twice daily. In the coronal projection shown, the axial images are viewed edge-on. The brain is clearly visible in the images due to the relatively long T_2 value and short self-diffusion coefficient of water relative to other anatomy. Also visible are the spleen, kidneys, and testes. However, most apparent are the changes in the bone marrow signal intensity after G-CSF administration. This was consistent with the known increased hematopoietic activity induced by G-CSF and confirmed by the elevation in white blood cell count from a baseline of $10 \times 10^3/\mu L$ to $71 \times 10^3/\mu L$ on day 5. The change in image intensity corresponded with a significant increase in the water T_2 value of the marrow. In the right posterior iliac crest the T_2 value increased from 43.7 ± 5.4 to 58.4 ± 4.9 msec, presumably due to the growing population of immature cells generated by the G-CSF. This was accompanied by a change in the apparent water fraction from 0.44 ± 0.06 to 0.69 ± 0.04 in the same region, suggesting an increase in the percentage cellularity. Also noted was a marked increase in the size of the spleen, from 238 to 493 mm^3 as measured by integrating regions of interest over the axial slices. An increase in splenic volume has previously been reported in some patients receiving G-CSF (12–14).

A second example is presented in Fig. 2 from a 28-year-old female patient with acute myelogenous leukemia. The coronal projection image shown in Fig. 2a was obtained prior to a course of myelosuppressive chemotherapy, which included cytarabine and idarubicin for a total of 5 days. At the time of the study, the white blood cell count was $40.5 \times 10^3/\mu L$. A bone marrow biopsy performed 4 days prior to the baseline MRI study demonstrated increased bone marrow cellularity and a differential count that included 36% myeloblasts. In the image much of the axial skeleton and proximal femora exhibit a strong signal intensity. The apparent water fraction was 0.99 ± 0.06, and the T_2 value of water was 61.7 ± 1.8 msec, consistent with the presence of leukemia (4). In addition, splenomegaly is evident. Of note, this patient had presented with a chloroma (a local collection of leukemia cells) in the left breast, which is also visible in the image, directly above the spleen. The patient was studied again 20 days after the start of therapy, after a complete remission (only 2% myeloblasts on the differential count) was confirmed by a repeat bone marrow aspiration. The corresponding image is shown in Fig. 2b. The signal from the bone marrow and spleen is almost completely absent, similar to that observed for normal bone marrow (4).

The third example, shown in Fig. 3, was obtained from a 76-year-old man with metastatic prostate cancer receiving docetaxel (35 mg/m^2/week, on a 3 weeks on/1 week off schedule) and estramustine (280 mg the nights before, of, and after docetaxel administration). The baseline scan was obtained 1 week prior to the start of therapy. A second scan was obtained during the 6th week of therapy and a third after 12 weeks of treatment. The maximum intensity projection images clearly show multiple focal lesions throughout the pelvis, as well as the lumbar and thoracic spine. Juxtaposed to the diffusion images are higher resolution STIR images obtained at the same time points. In Fig. 3 the maximum intensity projections were generated from coronal STIR data sets with slices covering only the vertebral bodies of the lumbar spine in order to facilitate a comparison of lesions visualized in this region with data

obtained from the diffusion-weighted images. Larger field-of-view STIR projections were limited by curvature of the spine and associated encroachment of signal from cerebro-spinal fluid. Over the three time points shown in Fig. 3, this patient's prostate-specific antigen levels, which are used as a measure of tumor activity, were 18, 26, and 32, respectively. While the STIR images also indicated tumor progression, the large, increasingly intense lesion in L2 on the STIR data sets nevertheless had calculated water self-diffusion coefficients equal to $D^* = 0.70 \pm 0.21$, 1.18 ± 0.25, and $1.43 \pm 0.30 \times 10^{-3}$ mm^2/sec for the three time points, respectively. The effect of increasing self-diffusion coefficients can be seen in Figs. 3a–c, where the lesion in L2 becomes progressively less intense relative to most lesions in neighboring thoracic and lumbar vertebrae.

DISCUSSION

An important aspect of the techniques described in this paper involves the specific utilization of simultaneous T_2 and diffusion weighting combined with spatial–spectral excitation of the water resonance to obtain the image contrast presented in the figures. The diffusion weighting tends to filter out extracellular fluid such as blood, CSF, and urine from the images. This is reasonable to expect since for self-diffusion coefficients close to that of free water the expected signal attenuation with $b = 1000$ sec/mm^2 was nearly a factor of 10, and the signal-to-noise ratio per voxel was also typically near 10. On the other hand the long T_2 weighting discriminated against water arising in muscle and many other organs. The most prevalent remaining signals arose from the bone marrow, brain, kidneys, prostate, and testes. The fact that bone marrow lesions were visible relative to normal bone marrow appears to be due to an increase in the water T_2 value coupled with an increase in cellularity as is common in neoplasia. The methods should thus be applicable to the broad classes of lesions exhibiting increased T_2 values on magnetic resonance images (15).

While it is the increased water T_2 values that facilitate the visualization of leukemia, it has been shown that the self-diffusion coefficient of water in bone marrow can change by as much as a factor of 3 after administration of ablative therapy, which directly affects the image according to Eq. [1] (4). This fact may render diffusion-weighted images more sensitive or at a minimum complementary to T_2-weighted images for therapeutic monitoring (16). In addition, the calculation of T_2, D^*, or other physical quantities responsible for the image contrast is useful whenever possible since in principle they can be made insensitive to variables associated with the data acquisition hardware such as coil sensitivity profiles and receiver gains. For example, in Fig. 3, the STIR images showed little therapeutic effect while the diffusion-weighted imaging data suggested a more mixed response. For lesions such as the one in L2, D^* was found to increase over the three studies. A traditional view of this finding suggests a tumor response by virtue of cell membrane compromise and a subsequent increase in the extracellular to intracellular water ratio (17). More recent work has also raised the possibility that water in different binding states may be an important contributing factor to self-diffusion coefficients in vivo (18,19). In this example it was also useful to compare the water self-diffusion coefficients in bone marrow with those obtained for brain parenchyma, which was expected to remain unaffected by the therapy. In the occipital cortex it was found that $D^* = 0.72 \pm 0.08$, 0.79 ± 0.10, and $0.75 \pm 0.11 \times 10^{-3}$ mm^2/sec at the three successive time points, indicating good system stability over the course of the exams.

The images in each of the figures are presented as static coronal maximum intensity projections for convenient visualization on the printed page. The projection methods are also amenable to direct comparison with complementary whole-body imaging techniques such as the bone scan. However, the three-dimensional rotating format was found to be much more useful for visualizing the extent of bone marrow disease, as well as for identifying image artifacts, such as those due to incomplete lipid suppression or image ghosting.

Since most anatomy of interest was within the trabecular bone, motion artifacts were minimal relative to other structures. In addition, although magnetic susceptibility differences at tissue–air and other interfaces do have the potential to degrade the echo-planar images due to the low bandwidth in the phase encoding direction, the use of axial slices minimized geometric distortion. Finally, the anatomy in the whole-body images can be used to advantage in volume quantification. For example, in the stem cell donor presented in Fig. 1, it was of interest to calculate the change in spleen size after G-CSF administration. Here the brain served as an internal volumetric calibration standard.

CONCLUSIONS

The techniques described above provide a potential means to rapidly evaluate therapeutic response in human bone marrow. A pathway to routine clinical implementation of the methods may exploit the potential for significant improvements in image quality or a reduction in the overall study time using multiple receive resonators in combination with parallel imaging techniques, higher magnetic field strengths, multishot, multiexcitation, echo-planar methods, and stronger, shorter gradient pulses in combination with shorter echo times.

Acknowledgements

The authors thank Josef Debbins and Bryan Mock of GE Medical Systems for helpful discussions.

Grant sponsor: National Heart, Lung and Blood Institute; Grant number: HL50139; Grant sponsor: National Institute of Biomedical Imaging and Bio-engineering; Grant number: EB002070; Grant sponsor: United States Army Medical Research and Materiel Command; Grant number: BC995795.

References

1. Naeim, F. Atlas of Bone Marrow and Blood Pathology. Philadelphia: Saunders; 2001. Normal bone marrow structure and blood cells; p. 1-13.
2. Castellino, RA. Imaging techniques in cancer management. In: DeVita, VT., Jr; Hellman, S.; Rosenberg, SA., editors. Cancer Principles & Practice of Oncology. 5. Philadelphia: Lippincott–Raven; 1997. p. 633-643.
3. Larson, SM. Radionuclide imaging. In: DeVita, VT., Jr; Hellman, S.; Rosenberg, SA., editors. Cancer Principles & Practice of Oncology. 5. Philadelphia: Lippincott–Raven; 1997. p. 663-669.
4. Ballon D, Dyke J, Schwartz LH, Lis E, Schneider E, Lauto A, Jakubowski AA. Bone marrow segmentation in leukemia using diffusion and T_2 weighted echo-planar imaging. NMR Biomed 2000;13:321–328. [PubMed: 11002312]
5. Glover GH, Schneider E. Three-point Dixon technique for true water/fat decomposition with B_0 inhomogeneity correction. Magn Reson Med 1991;18:371–383. [PubMed: 2046518]
6. Ballon D, Jakubowski A, Gabrilove J, Graham MC, Zakowski M, Sheridan C, Koutcher JA. *In vivo* measurements of bone marrow cellularity using volume localized proton NMR spectroscopy. Magn Reson Med 1991;19:85–95. [PubMed: 2046540]
7. Stejskal EO, Tanner JE. Spin diffusion measurements: spin echoes in the presence of time-dependent field gradients. J Chem Phys 1965;42:288–292.
8. Mirowitz SA, Apicella P, Reinus WR, Hammerman AM. MR imaging of bone marrow lesions: relative conspicuousness on T_1-weighted, fat-suppressed T_2-weighted, and STIR images. Am J Roentgenol 1994;162:215–221. [PubMed: 8273669]
9. Pauly J, Spielman D, Macovski A. Echo-planar spin-echo and inversion pulses. Magn Reson Med 1993;29:776–782. [PubMed: 8350720]
10. Schick F, Forster J, Machann J, Kuntz R, Claussen CD. Improved clinical echo-planar MRI using spatial-spectral excitation. J Magn Reson Imaging 1993;8:960–967. [PubMed: 9702899]
11. Ballon D, Jakubowski A, Tulipano PK, Graham MC, Schneider E, Aghazadeh B, Chen QS, Koutcher JA. Quantitative assessment of bone marrow hematopoiesis using parametric magnetic resonance imaging. Magn Reson Med 1998;39:789– 800. [PubMed: 9581611]

12. Platzbecker U, Prange-Krex G, Bornhauser M, Koch R, Soucek S, Aikele P, Haack A, Haag C, Schuler U, Berndt A, Rutt C, Ehninger G, Holig K. Spleen enlargement in healthy donors during G-CSF mobilization of PBPCs. Transfusion 2001;41:184–189. [PubMed: 11239220]

13. Stroncek D, Shawker T, Follmann D, Leitman SF. G-CSF-induced spleen size changes in periperhal blood progenitor cell donors. Transfusion 2003;43:609– 613. [PubMed: 12702182]

14. Picardi M, De Rosa G, Selleri C, Scarpato N, Soscia E, Martinelli V, Ciancia R, Rotoli B. Spleen enlargement following recombinant human granulocyte colony stimulating factor administration for peripheral blood stem cell mobilization. Haematologica 2003;88:794– 800. [PubMed: 12857559]

15. Vanel, D.; Tardivon, AA. Bone marrow cancer. In: Stark, DD.; Bradley, WG., editors. Magn Reson Imaging. 3. St Louis: Mosby; 1999. p. 977-987.

16. Byun WM, Shin SO, Chang Y, Lee SJ, Finsterbusch E, Frahm J. Diffusion-weighted MR imaging of metastatic disease of the spine: assessment of response to therapy. Am J Neuroradiol 2002;23:906–912. [PubMed: 12063214]

17. Van Zijl PC, Moonen CT, Faustino P, Pekar J, Kaplan O, Cohen JS. Complete separation of intracellular and extracellular information in NMR spectra of perfused cells by diffusion-weighted spectroscopy. Proc Natl Acad Sci USA 1991;88:3228–3232. [PubMed: 2014244]

18. Schwarcz A, Bogner P, Meric P, Correze JL, Berente Z, Pál J, Gallyas F, Doczi T, Gillet B, Beloeil JC. The existence of biexponential signal decay in magnetic resonance diffusion-weighted imaging appears to be independent of compartmentalization. Magn Reson Med 2004;51:278–285. [PubMed: 14755652]

19. Maier SE, Vajapeyam S, Mamata H, Westin CF, Jolesz FA, Mulkern RV. Biexponential diffusion tensor analysis of human brain diffusion data. Magn Reson Med 2004;51:321–330. [PubMed: 14755658]

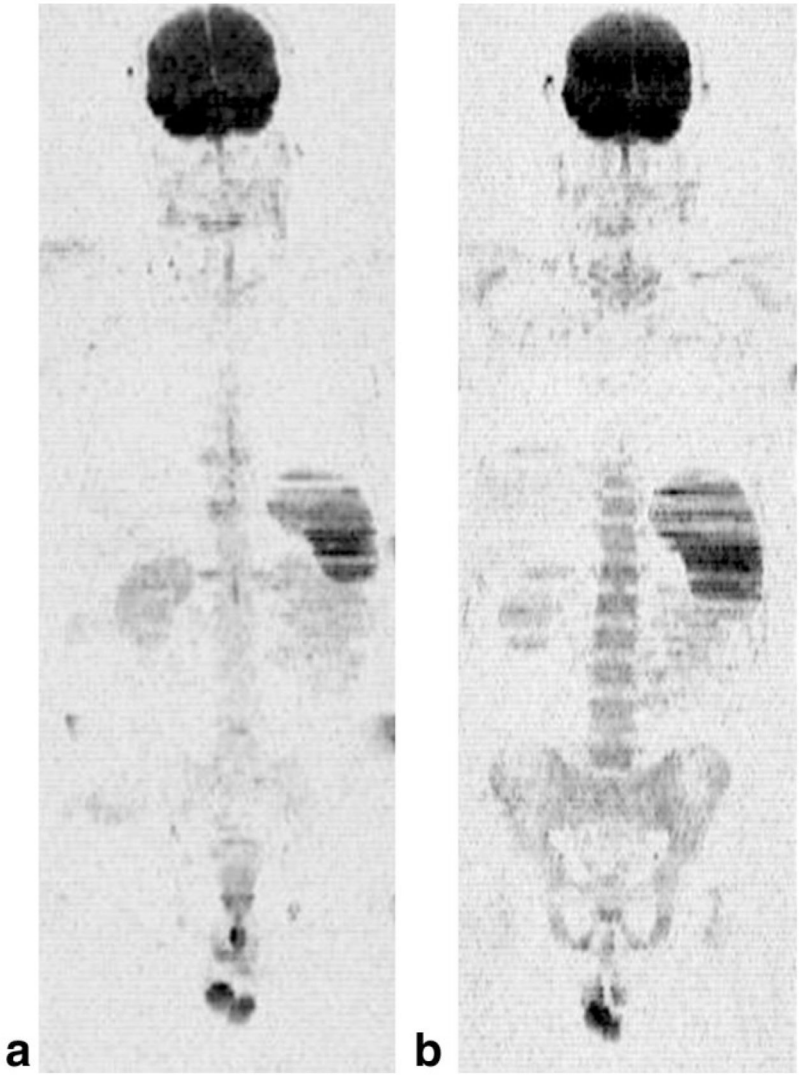

FIG. 1.

Coronal maximum intensity projections from three-dimensional data sets of diffusion-weighted images obtained from a normal adult receiving granulocyte colony-stimulating factor prior to stem cell harvest and donation to a sibling with leukemia: (**a**) Day 0 and (**b**) Day 5 of G-CSF administration. The signal from bone marrow in the axial skeleton is markedly increased, consistent with a change in both the apparent water fraction, from 0.44 ± 0.06 to 0.69 ± 0.04, and the T_2 value of water in the marrow, from 43.7 ± 5.4 to 58.4 ± 4.9 msec. The spleen also increased in size, from 238 to 493 mm^3. The white blood cell count underwent a sevenfold increase over the same time period. The results are consistent with bone marrow mobilization.

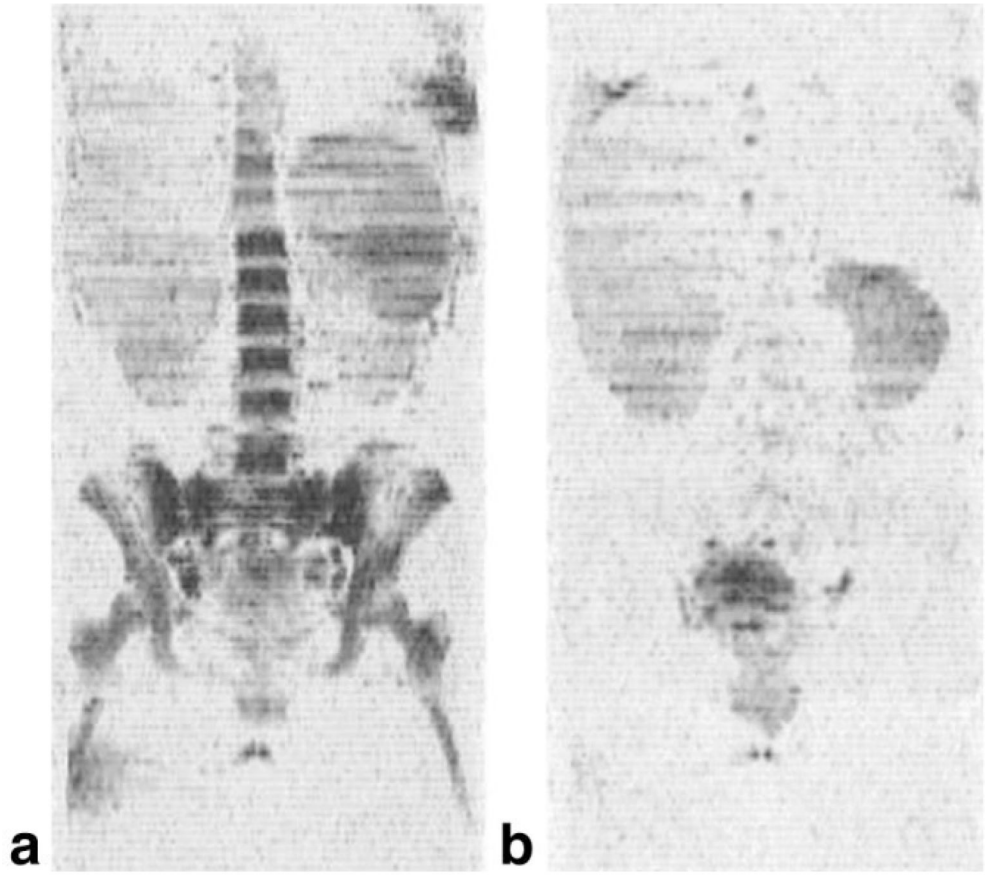

FIG. 2.

The techniques applied to a subject with acute myelogenous leukemia: (**a**) coronal image from a baseline study obtained just prior to initiation of myelosuppressive therapy, (**b**) a second examination obtained 20 days later after the patient had achieved a remission. The bone marrow was intact at baseline with a water fraction of 0.99 ± 0.06 and a T_2 of water equal to 61.7 ± 1.8 msec, which is consistent with the presence of leukemia. Twenty days after the start of chemotherapy, the water signal in the bone marrow on the T_2- and diffusion-weighted images is virtually absent. The patient had achieved a complete remission at this time, with only 2% myeloblasts on the differential blood count.

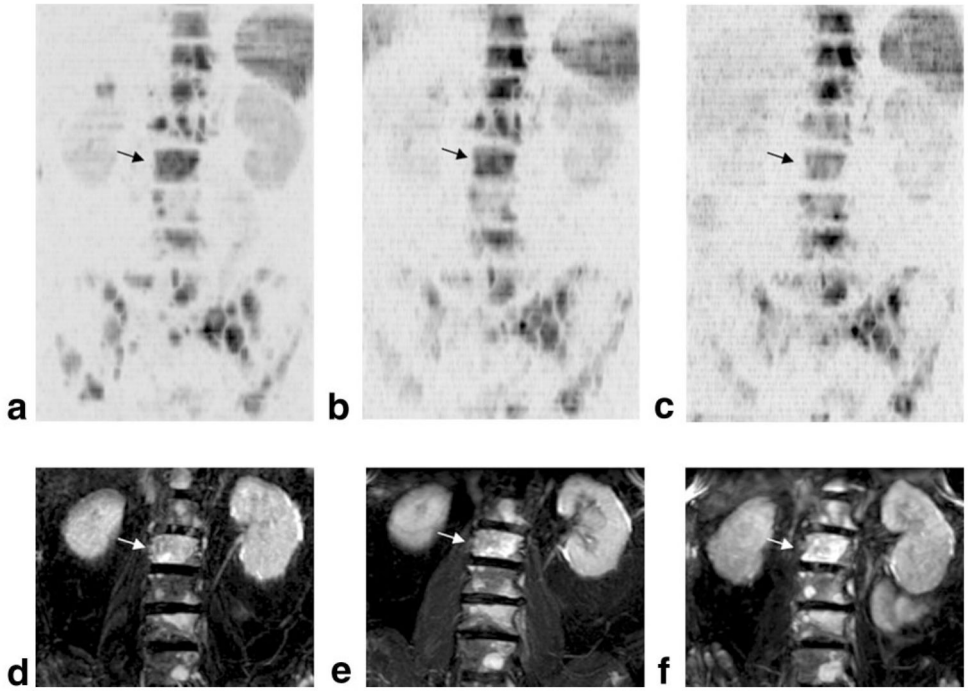

FIG. 3.

Data from a 76-year-old man with prostate cancer metastatic to bone. Coronal maximum intensity projection images are shown at (**a**) 1 week prior to the start of chemotherapy, (**b**) during week 6, and (**c**) after 12 weeks of therapy. (**d–f**) Corresponding maximum intensity projection images of the lumbar spine generated from a STIR data set at the same time points. Because of overlapping signals in the STIR data set from cerebrospinal fluid, only coronal slices intersecting the lumbar spine anterior to the vertebral foramina were included. The lesion in L2 denoted by dark arrows on the diffusion-weighted series and light arrows on the STIR series suggests a more positive response to therapy than most other lesions (see text for details).